

# Competition between ocean carbon pumps in simulations with varying Southern Hemisphere westerly wind forcing

W. N. Huiskamp<sup>1,2</sup> · K. J. Meissner<sup>1,2</sup> · M. d'Orgeville<sup>3</sup>

Received: 26 February 2015 / Accepted: 23 July 2015  
© Springer-Verlag Berlin Heidelberg 2015

**Abstract** We analyse the impact of migration and strength of Southern Hemisphere westerly winds on the ocean carbon cycle in a systematic sensitivity study with the University of Victoria Earth System Climate Model. We find that changes in the biological pump are mainly driven by changes in ocean residence times while changes in export production are negligible. Changes in the biological and physical pumps are always of opposite sign; with the physical pump being dominant for southward shifts and the biological pump being dominant for northward shifts. Furthermore, changes in the Pacific Ocean carbon budget dictate the overall changes in global marine and atmospheric carbon. Overall, atmospheric CO<sub>2</sub> increases (and Δ<sup>14</sup>C decreases) for northward shifts or a strengthening in wind forcing. The opposite is true for a southward shift or a weakening in wind forcing. Combining forcings (shift and intensity change) results in a combination of their impacts with the direction of the shift being the first order forcing. The terrestrial carbon reservoir absorbs (releases) 50–70 % of the net oceanic carbon loss (increase), counterbalancing the effect on atmospheric CO<sub>2</sub>.

**Keywords** Carbon cycle · Southern Hemisphere westerlies · Southern annular mode · Ocean dynamics · Preformed and remineralized DIC

✉ W. N. Huiskamp  
willemhuiskamp88@gmail.com; w.huiskamp@unsw.edu.au

<sup>1</sup> Climate Change Research Centre, UNSW Australia, Sydney, NSW, Australia

<sup>2</sup> ARC Centre of Excellence for Climate System Science, UNSW Australia, Sydney, NSW, Australia

<sup>3</sup> Department of Physics, University of Toronto, Toronto, Ontario, Canada

## 1 Introduction

The Southern Hemisphere westerly wind belt is the region at around 50°S of annual mean maximum surface wind speed that plays an important role in deep and intermediate water formation, upwelling, as well as gas exchange in the Southern Ocean. The Southern Ocean is currently a net carbon sink of approximately 1 Pg C/year (Takahashi et al. 2012; Sasse et al. 2013), roughly 50–70 % of the global ocean carbon sink, significantly offsetting the rate of net atmospheric CO<sub>2</sub> increase due to anthropogenic activities. The Southern Hemisphere westerlies (SHW) have undergone a poleward shift since the 1970's (Russell et al. 2006), due to both anthropogenic warming and decreasing stratospheric ozone (Son et al. 2008; Lee and Feldstein 2013; Previdi and Polvani 2014). It has been hypothesised that such a poleward shift of the SHW may enhance the Southern Ocean's ability to remove CO<sub>2</sub> from the atmosphere (Russell et al. 2006; Zickfeld et al. 2007; Tschumi et al. 2008; Huiskamp and Meissner 2012) or, on the contrary, result in increased ventilation of old and carbon-rich water from the deep ocean (Toggweiler et al. 2006; Skinner et al. 2010).

For example, Russell et al. (2006) and Zickfeld et al. (2007) studied the response of global oceanic and terrestrial carbon sinks to projected changes in the SHW due to anthropogenic forcing. Zickfeld et al. (2007) find that a southward shift and intensification of the SHW under increasing CO<sub>2</sub> forcing results in a relatively small decrease in atmospheric CO<sub>2</sub> of 9 Pg C over the period 1900–2100, during which most of the carbon is exchanged between the ocean and terrestrial biosphere. Russell et al. (2006) find a similar result, with a southward shift and intensification of the SHW enhancing the ocean's ability to absorb CO<sub>2</sub> and heat in their simulations. This is due to decreased

stratification south of the sub-antarctic front and hence, a more ventilated Southern Ocean. Publications based on the opposite mechanism (a southward migration of SHW leading to an increase in atmospheric CO<sub>2</sub> and vice-versa), are either based on conceptual models (Skinner et al. 2010) or simplified ocean models (Toggweiler et al. 2006).

The ventilation and uptake of carbon has been found to be more sensitive to changes in the intensity of wind stress than to latitudinal shifts (Tschumi et al. 2008; d'Orgeville et al. 2010), while latitudinal location can control the exchange of carbon between ocean basins (Huiskamp and Meissner 2012) or between deep and intermediate water masses (d'Orgeville et al. 2010). For example, a decrease in SHW intensity has been related to a decreased ventilation of the Southern Ocean due to less frequent and shallower convective events (Tschumi et al. 2008). This decreased ventilation of the deep Southern Ocean results in a decrease in atmospheric CO<sub>2</sub>, with the opposite being true for increased intensity (Tschumi et al. 2008; d'Orgeville et al. 2010).

Finally, the SHW are also thought to impact North Atlantic Deep Water (NADW) formation (Delworth and Zeng 2008; Sijp and England 2009; Völker and Köhler 2013) via changes in northward surface transport and Agulhas leakage (Biastoch et al. 2009). The 'Drake Passage effect' hypothesises that the magnitude of zonal wind stress at the latitude of the Drake Passage controls the magnitude of NADW leaving the Atlantic basin (Toggweiler and Samuels 1995). It has been shown to link increases in SHW intensity to increases in NADW formation and vice versa (McDermott 1996; Rahmstorf and England 1997; Delworth and Zeng 2008). For example, simulations forced with northward shifted westerlies during the last glacial period (Sijp and England 2008) and subsequent deglaciation (Huiskamp and Meissner 2012) show a significant reduction in NADW formation due to reduced Agulhas leakage which leads to a cooling and freshening of the thermocline, intermediate and mode waters in the Atlantic Ocean in the UVic Earth System Climate Model (ESCM) (Sijp and England 2008).

It should be noted that these previous studies have been conducted under different forcing and boundary conditions, which makes consistent comparisons difficult. Sijp and England (2008), Sijp and England (2009), d'Orgeville et al. (2010) and Huiskamp and Meissner (2012) perturbed the wind stress only, thereby isolating the dynamic forcing on the ocean; whereas Zickfeld et al. (2007) and Menzel et al. (2008) changed both wind stress and surface wind speed, which is used in the calculation of ocean-atmosphere fluxes of heat and fresh water. The boundary conditions vary from glacial (Völker and Köhler 2013); deglacial (Huiskamp and Meissner 2012); preindustrial (Tschumi et al. 2008; Sijp and England 2008, 2009; d'Orgeville et al. 2010) to

future climate (Zickfeld et al. 2007; Russell et al. 2006). Furthermore, transient responses in the ocean carbon sink to changes in the westerlies (Zickfeld et al. 2007; Russell et al. 2006; Huiskamp and Meissner 2012) may differ from fully equilibrated sensitivity studies such as Tschumi et al. (2008), d'Orgeville et al. (2010), Völker and Köhler (2013). Finally, most studies analyse the impact of changes in Southern Hemisphere westerly winds on the natural carbon cycle, while a few include both, natural and anthropogenic carbon in their analysis (Zickfeld et al. 2007; Russell et al. 2006). Lovenduski et al. (2007) and Lovenduski and Ito (2009) separate natural and anthropogenic carbon in their analysis of air-sea fluxes with biogeochemical enabled versions of the MIT general circulation model (gcm) and the Parallel Ocean Program (POP) model.

The ability of the SHW to affect global climate via changes in atmospheric CO<sub>2</sub>, ocean circulation and heat transport, as well as the contradicting predictions on how future changes in the SHW will impact atmospheric CO<sub>2</sub> concentrations, highlights the need for a detailed sensitivity study.

This study therefore aims to build on earlier research by conducting a broad sensitivity study spanning the parameter space of both intensity and latitudinal location of the SHW wind stress and their impact on the carbon cycle under preindustrial boundary conditions. Changes in ocean carbon are deconstructed into physical and biogeochemical mechanisms in order to analyse the impact of changing SHW on the ocean carbon pool.

## 2 Methods

This study utilises the University of Victoria Earth System Climate Model (UVic ESCM) version 2.9, which consists of a series of sub-models coupled together for relevant feedbacks between them. The ocean is represented by the Modular Ocean Model, Version 2 (Pacanowski 1995), an ocean general circulation model with 19 vertical levels. Ocean diffusivity in the horizontal is  $k_h = 8 \times 10^2 \text{ m}^2 \text{ s}^{-1}$  and in the vertical varies from thermocline  $k_v = 0.3 \times 10^{-4} \text{ m}^2 \text{ s}^{-1}$  to deep ocean  $k_v = 1.3 \times 10^{-4} \text{ m}^2 \text{ s}^{-1}$  (after Bryan and Lewis (1979)). Mesoscale eddies are parameterised using the Gent and McWilliams scheme (Gent and McWilliams 1990) with a constant eddy thickness diffusivity in time and space of  $800 \text{ m}^2 \text{ s}^{-1}$ . The ocean model is coupled to a vertically integrated, two dimensional energy-moisture balance model of the atmosphere. In addition to these, the UVic ESCM includes a dynamic-thermodynamic sea ice model derived from Semtner (1976), Hibler (1979) and Hunke and Dukowicz (1997), a sediment model (Archer 1996; Meissner et al. 2012), a land surface scheme and a dynamic global vegetation model (Meissner et al. 2003a). The UVic ESCM

also includes an improved NPZD (nutrient, phytoplankton, zooplankton and detritus) model with a parameterisation of rapid nutrient recycling due to microbial activity (Schartau and Oschlies 2003). The NPZD model contains two classes of phytoplankton, nutrients (nitrate and phosphate) and the prognostic tracers of oxygen, dissolved inorganic carbon (DIC) and alkalinity (Schmittner et al. 2008). To distinguish between the biological and physical pumps, we have introduced two additional prognostic tracers that explicitly track preformed and remineralised DIC (Chen and Millero 1979) and sum to total DIC in the ocean ( $DIC_{tot} = DIC_{rem} + DIC_{pref}$ ; see Ito and Follows (2005), Equations 5–8). All DIC in the surface layer of the ocean is defined as preformed carbon ( $DIC_{tot}(\text{surface}) = DIC_{pref}(\text{surface})$ ). Preformed DIC therefore includes the saturation state of the ocean, which is sensitive to changes in  $pCO_2$ , surface alkalinity, salinity, and temperature, as well as the disequilibrium term accounting for the finite time scale of air-sea exchange ( $DIC_{pref} = DIC_{sat} + DIC_{dis}$ ).  $DIC_{pref}$  is then transported to deeper layers via circulation, while the  $DIC_{rem}$  tracer keeps track of new DIC formed by remineralisation of organic carbon at depth, including carbon from both the soft tissue and the carbonate pump ( $DIC_{rem} = DIC_{soft} + DIC_{carb}$ ). These two prognostic tracers were included for the full integration time of 7,000 years. A more thorough description of the physical components of the model can be found in Weaver et al. (2001).

The model is driven by insolation at the top of the atmosphere in addition to wind stress and wind fields for transport of heat and moisture (Kalnay et al. 1996), both of which vary seasonally. All model components have a resolution of 3.6 degrees in longitude and 1.8 degrees in latitude. During simulations, the model conserves water, energy and carbon to machine precision. Comparisons of the model's results with observations and proxy data show good agreement, examples are Weaver et al. (2001), Meissner et al. (2003a, b) and Eby et al. (2009).

The control simulation was integrated under preindustrial boundary conditions (orbital parameters corresponding to year 1800 (Berger 1978), atmospheric  $CO_2$  of 280 ppm and present day winds) for a period of 16,500 years. At the end of the integration, the global  $^{14}C$  flux into the ocean was diagnosed and this flux was set equal to the production rate in the atmosphere, allowing the model to calculate  $^{14}C$  prognostically (Meissner et al. 2003b; Meissner 2007). The wind stress field between  $25^{\circ}S$  and  $90^{\circ}S$  was shifted by 1.8, 3.6 or 5.4 degrees north- or south-ward. In addition, a 5.4 degrees latitude buffer zone was created to avoid discontinuities at the boundary. A linear transition between altered fields and climatology was applied in the buffer zone. Changes in intensity ( $\pm 20\%$ ) and combinations of these forcings (Fig. 1a; Table 1) were also conducted. These sensitivity simulations were integrated to

equilibrium for an additional 7000 years, after which the last 100 years of each simulation were averaged and used for analysis. Both the zonal and meridional components of the wind stress are changed in our simulations. Simulations are named after the magnitude of the latitudinal shift followed by the change in intensity. For example, simulation 3N-12 is forced with westerly winds shifted north by  $3 \times 1.8^{\circ}$  ( $= 5.4^{\circ}$ ) in latitude and a 20 % increase in intensity (1.2 times the original intensity). Similarly, simulation 0-08 is forced by winds without a latitudinal shift and a 20 % reduction in intensity.

To analyse changes in the ventilation of different water masses, additional dye tracer simulations were integrated for 1000 years using the end-members of each simulation. The concentration of each dye tracer is set equal to 1 in the surface layer of a given region at each timestep (Fig. 1b)

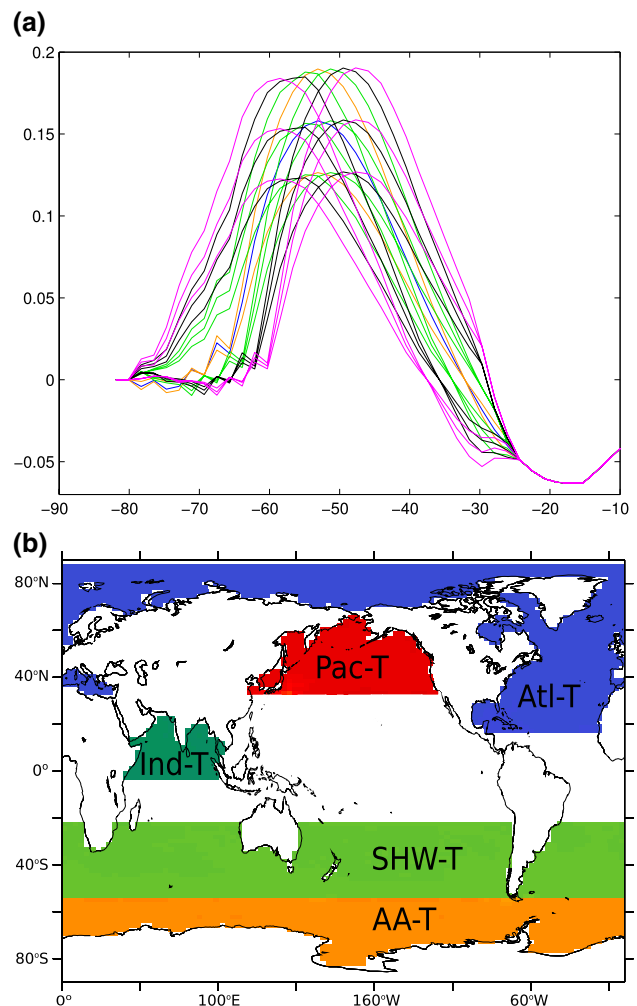


**Fig. 1** **a** Zonal and annual mean wind stress fields (Pa) and **b** regions of artificial dye tracers

**Table 1** List of simulations

Name	SHW shift North (°)	SHW shift South (°)	Intensity change (%)	Symbol
0-08	–	–	20	*
0-12	–	–	+20	+
1N-0	1.8	–	–	◊
1N-08	1.8	–	20	*
1N-12	1.8	–	+20	+
1S-0	–	1.8	–	○
1S-08	–	1.8	20	*
1S-12	–	1.8	+20	+
2N-0	3.6	–	–	◊
2N-08	3.6	–	20	*
2N-12	3.6	–	+20	+
2S-0	–	3.6	–	○
2S-08	–	3.6	20	*
2S-12	–	3.6	+20	+
3N-0	5.4	–	–	◊
3N-08	5.4	–	20	*
3N-12	5.4	–	+20	+
3S-0	–	5.4	–	○
3S-08	–	5.4	20	*
3S-12	–	5.4	+20	+

Wind stress fields of the Southern Hemisphere Westerlies (SHW) are shifted northward, southward or remain in their present day location. The intensity of the field is either increased or decreased by 20 %, or remains at present day values

and is reset to 0 if it subsequently reaches the surface layer again in a different region.

### 3 Results

#### 3.1 Atmospheric, ocean and terrestrial carbon budgets

Globally averaged ocean ventilation rates can be inferred from changes in atmospheric  $^{14}\text{C}$ , a radionuclide formed in the upper atmosphere with a half life of  $5730 \pm 40$  years and commonly expressed as  $\Delta^{14}\text{C}$ , a standardised ratio of  $^{14}\text{C}$  to the stable  $^{12}\text{C}$  (Stuiver and Polach 1977). When the

production rate is known, changes in atmospheric  $^{14}\text{C}$  can be related to the exchange of  $^{14}\text{C}$  between the atmosphere and 'old' ( $^{14}\text{C}$  depleted) carbon reservoirs; primarily the deep and intermediate water masses of the ocean. If deep ocean ventilation increases, we expect a decrease in atmospheric  $\Delta^{14}\text{C}$  as  $^{14}\text{C}$  depleted carbon enters the atmosphere, while the opposite is true for a decrease in ventilation. Changes in atmospheric  $\text{CO}_2$  versus changes in atmospheric  $\Delta^{14}\text{C}$  with respect to the control simulation are shown in Fig. 2a. The near linear relationship between the two indicates that the mean age of carbon reservoirs (in terms of  $\Delta^{14}\text{C}$ ) exchanging with the atmosphere is almost constant.

As shown in Fig. 2a, a southward shift of the wind stress field results in a decrease in atmospheric  $\text{CO}_2$  and an increase in atmospheric  $\Delta^{14}\text{C}$ , with the opposite being broadly true for northward shifts (northward shifts are indicated by green diamonds in Fig. 2a, b). An analysis of anomalies in dissolved inorganic carbon (DIC) suggest a seesaw relationship between the "Atlantic-northern Southern Ocean" and "Pacific-Indian-southern Southern Ocean" basins (Fig. 3). For northward shifts of the SHW (upper panels), the Pacific and Indian basins as well as the Southern Ocean south of  $60^\circ\text{S}$  lose carbon while the Atlantic basin as well as the Southern Ocean north of  $60^\circ\text{S}$  gain carbon. The Atlantic basin accumulates a maximum of 100 PgC while the Pacific Basin loses a maximum of 176 PgC (simulation 3N-12). At the same time carbon is outgassed to the atmosphere, with a net atmospheric gain of 40.5 PgC for simulation 3N-12. Southward shifts result in an increase in total ocean carbon in agreement with Russell et al. (2006). DIC anomalies for southward shifts of the SHW are broadly of the opposite sign and smaller than what occurs during northward shifts. The Atlantic basin loses a maximum of 22 PgC (simulation 1S-08) and the Pacific accumulates a maximum of 69 PgC (simulation 3S-08).

A weakening of the SHW by 20 % results in a decrease in atmospheric  $\text{CO}_2$  of 4 ppm while a strengthening leads to an increase of 6 ppm which is in broad agreement with previous studies (Russell et al. 2006; Tschumi et al. 2008; d'Orgeville et al. 2010). The combination of shifts and changes in intensity results in a combination of their respective impacts on the atmospheric  $\text{CO}_2$  signal. For example, while a southward shift of the SHW alone leads to a decrease in atmospheric  $\text{CO}_2$  and an increase in intensity alone leads to an increase, combining the two results in a scenario where the direction of the shift generally dominates but is partially mitigated by the change in intensity (Fig. 2a). This explains why simulations 1N-08 and 2N-08 stand out with a net decrease in atmospheric  $\text{CO}_2$ . For example, in simulation 1N-08, the effect of shifted winds is balanced by the decrease in intensity leading to little to no carbon being exchanged between the ocean and

atmosphere (Fig. 2b). Total soil carbon increases in this simulation due to an intensification and expansion of permafrost on Taymyr Peninsula in Russia. This results in a net decrease in atmospheric carbon.

The land surface and vegetation plays a non-negligible role as a carbon sink or source, not only for simulation 1N-08. The land surface absorbs 50–75 % of the carbon ventilated by the ocean (Figs. 2b, 4a) and vice versa. The terrestrial carbon cycle therefore partially compensates for any SHW induced change in atmospheric CO<sub>2</sub> in agreement with Zickfeld et al. (2007). For example, an increase in terrestrial carbon for northward shifted SHW simulations is caused by enhanced net primary productivity, which is mainly due to increased atmospheric CO<sub>2</sub> (Fig. 4b). The increased vegetation and soil carbon is partially counterbalanced by increased soil respiration due to higher soil temperatures. The opposite is true for southward shifts: a decrease in atmospheric CO<sub>2</sub> leads to a decrease in photosynthesis and a net loss of terrestrial carbon to the atmosphere; partially mitigating the direct effect of the winds on the ocean carbon budget.

### 3.2 Ocean circulation

Changes in ocean circulation and ventilation are examined to better understand the changes seen in oceanic DIC described above (Fig. 3). As the Southern Ocean is zonally unbounded at the latitude of the Drake Passage, no east–west pressure gradient and therefore, no geostrophic poleward flow can be maintained at this latitude. As a result, northward flowing surface waters in the Ekman layer must be balanced at depth where bathymetric features exist to accommodate a geostrophically balanced poleward flow. This is known as the Drake Passage effect (Toggweiler and Samuels 1995) and this return flow brings waters from the mid-depth (2–3 km) of the ocean to the surface, an important mechanism in the ventilation of deep, carbon rich water and one that is unique to the Southern Ocean (Russell et al. 2006).

The pre-industrial control simulation forms 21 Sv of North Atlantic Deep Water (NADW) and 11 Sv of Antarctic Bottom Water (AABW) (Fig. 5e). By increasing the intensity of the SHW (simulation 0–12), we find an intensification of northward Ekman transport, enhanced upwelling of circumpolar deep water at the Antarctic divergence and an increase in the depth from which water is upwelled (Fig. 5b), resulting in a more ventilated Southern Ocean; in agreement with Tschumi et al. (2008), d'Orgeville et al. (2010). The tilt of density surfaces induced by winds is balanced through the baroclinic instability of the thermal wind currents, which acts to flatten out the density surfaces and to transport mass polewards (Marshall and Speer 2012). The resulting mesoscale eddies are not resolved in

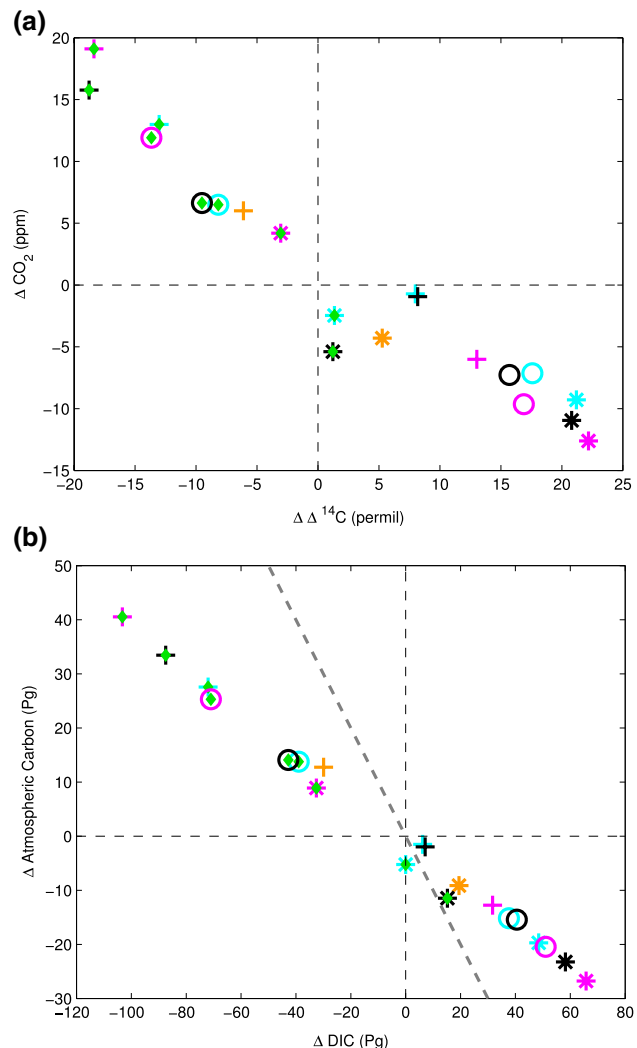


**Fig. 2** **a** Change in annual-mean atmospheric  $\Delta^{14}\text{C}$  versus  $\Delta\text{CO}_2$  with respect to the control simulation and **b** change in annual-mean atmospheric carbon versus globally integrated ocean DIC with respect to the control simulation ( $y = -x$  included in dashed grey). Cyan, black, magenta and orange represent simulations forced with shifted SHW by 1.8, 3.6, 5.4° and no shift in latitude respectively, while '+' denotes simulations forced with a 20 % increase in SHW intensity and '\*' denotes simulations with a 20 % decrease in intensity. Green diamonds indicate simulations forced with a northward shift. See also Table 1

our coarse resolution ocean model, they are parameterized via the Gent and McWilliams (1990) isopycnal diffusion scheme. It should be noted that the simulated residence time of water masses critically depends on the balance of these two opposing cells. For example, previous studies using either a high resolution idealised sector version of the MITgcm (Munday et al. 2014), the global version of the MIT general circulation and biogeochemistry model (Lauderdale et al. 2013) or the UVic ESCM (Swart et al. 2014) have shown that the effect of wind stress changes on Southern Ocean overturning and carbon storage is reduced when

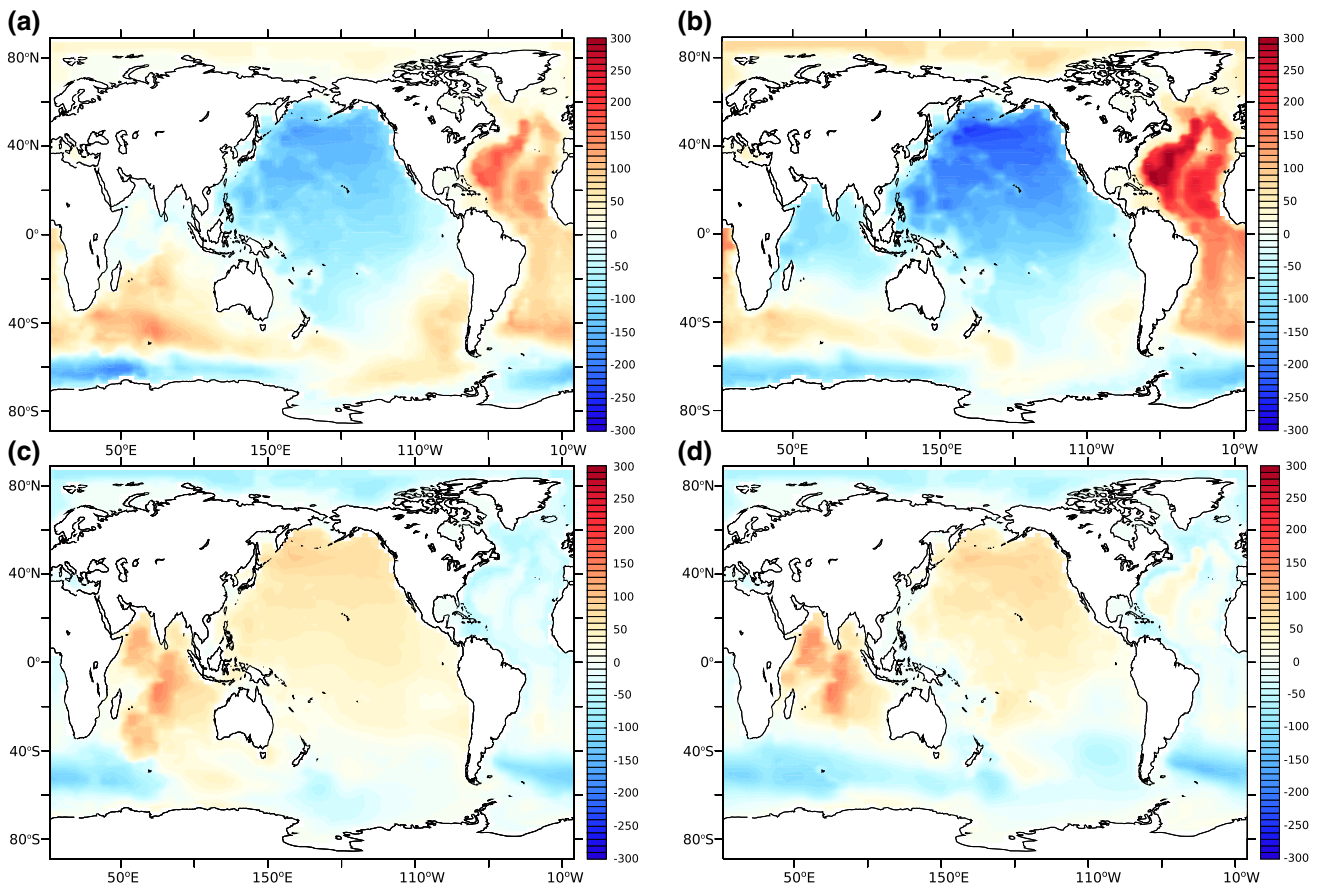


**Fig. 3** Change in annual-mean vertically integrated DIC ( $\text{mol m}^{-2}$ ) for simulations 3N-08 (a), 3N-12 (b), 3S-08 (c) and 3S-12 (d)

eddies are resolved or a spatially and temporally varying GM parameterisation is employed. Based on these previous studies, our simulations likely overestimate the sensitivity of the ocean carbon sink. Changes in ocean carbon for simulation 0–12 are primarily driven by a depletion in DIC in the top 2000 m of the Pacific basin as a result of enhanced Antarctic intermediate water (AAIW) formation. The opposite is true for experiment 0–08, in which DIC accumulates in the top 2000 m, accompanied by a weakening in AABW and AAIW formation (Fig. 5a).

As the Southern Ocean connects all of Earth's ocean basins, changes in the latitudinal position of the SHW have the potential to alter the exchange of heat and salt between basins. Similar to Sijp and England (2009), simulations forced with northward shifted SHW show a contraction of subpolar gyres in the Southern Hemisphere, a breakdown of the Atlantic-Indian Ocean supergyre, as well as a reduction in Agulhas leakage. Under present day conditions, the Agulhas current retroflects around the southern tip of South Africa and sheds eddies known as Agulhas rings into the South Atlantic. These eddies provide the Atlantic Ocean with warm, saline Indian Ocean water. If the SHW

are shifted northward, Agulhas leakage is impeded by increased eastward surface flow. The transport of salt from the Indian to the Atlantic Ocean decreases and results in a freshening of the Atlantic basin in our simulations. Over longer time-scales this leads to a decrease in North Atlantic Deep Water (NADW) formation of up to 5.5 Sv (Fig. 5c) due to a freshening of the high latitude North Atlantic; corroborating the studies of Delworth and Zeng (2008) and Sijp and England (2008) (Fig. 6b). The Indian and Pacific basins become more saline in these scenarios and an enhanced shallow thermohaline circulation in the North Pacific is established at depths between 500–1500 m, similar to Sijp and England (2009) (Fig. 6d).

The opposite is broadly true for southward shifts of the SHW, which lead to increased Agulhas leakage (Biasotocchi et al. 2009) and a decrease in ventilation in the North Pacific (Fig. 6d). Contrary to previous studies (d'Orgeville et al. 2010; Sijp and England 2009; Völker and Köhler 2013), simulations forced with southward shifted SHW result in a minor decrease in NADW formation of up to 1.5 Sv in our simulations instead of an increase (Figs. 5d, 6b). This is due to an increase in southern sourced water

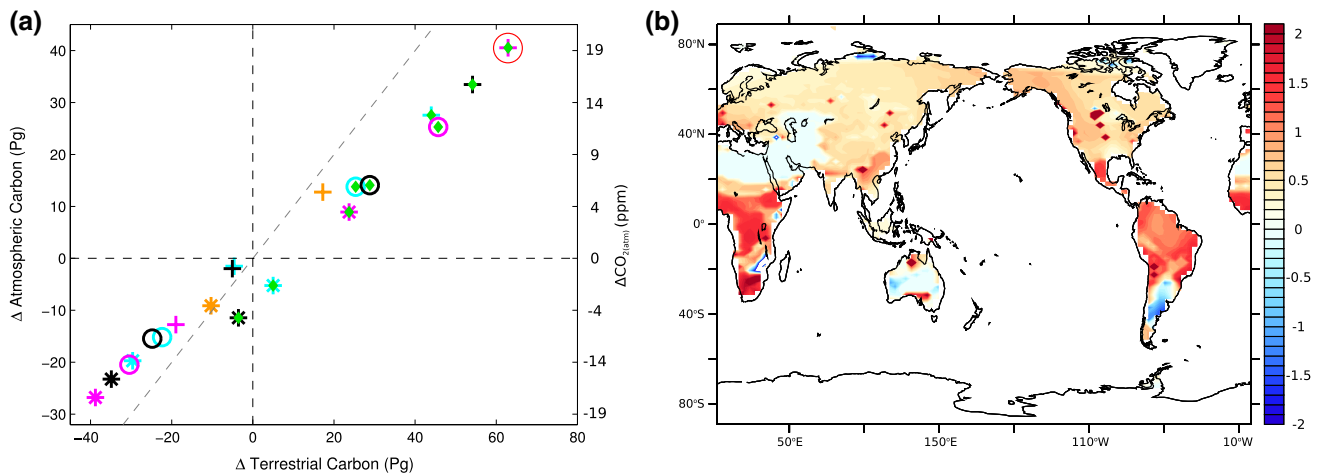


**Fig. 4** **a** Anomalies in annual mean atmospheric CO<sub>2</sub> (ppm/Pg) versus annual mean terrestrial carbon (Pg); x = y line in grey and **b** net primary production for simulation 3N-12 (highlighted on **a**) minus the control simulation ( $10^{-9} \text{ kg m}^{-2} \text{ s}^{-1}$ )

masses as discussed below, which leads to a weakening and shoaling of NADW; an example of the bipolar seesaw [e.g. Weaver and Hughes (1992), Saenko et al. (2003)].

Surprisingly, almost all simulations show an increase in global ocean ventilation when compared to the control simulation (Fig. 6a), driven primarily by Antarctic-sourced water masses (Fig. 6c). AABW is formed in the Weddell and Ross seas (Fig. 7g) in the control simulation. In simulations forced with a northward shift of the SHW, sea ice thickness increases, particularly in the Weddell Sea, resulting in a subsequent shift in location of deep water formation to 70°E off the coast of Mac. Robertson Land (Fig. 7a). A southward shift of the SHW leads to a decrease in sea ice thickness everywhere except for the Weddell Sea; resulting in decreased AABW formation in the Weddell Sea and enhanced AABW formation at 120°E near Wilkes Land (Fig. 7d). Southern sourced water mass formation rates therefore increase for both directions of wind shifts due to the appearance of two new deep water formation sites in addition to those operating in the control simulation. An important consequence of increased AABW formation for both north- and south-ward shifts is a decrease in global mean ocean temperatures; up to  $-0.7^{\circ}\text{C}$  for north- and up to  $-1.4^{\circ}\text{C}$  for southward shifts. This is important when considering changes in the efficiency of the physical pump, as discussed in Sect. 3.3.

To understand if these additional deep water formation sites are caused by either changes in ocean or changes in sea ice dynamics (or both), we integrated four additional simulations to separate the dynamic wind forcing on ocean and sea ice. Two “ICE” simulations investigate the role of ice dynamics: based on experiments 3N-0 and 3S-0, only the sea ice model is forced by the perturbed wind stress field, while the ocean model is forced by control winds (Fig. 7,

middle column). The opposite scenario (where perturbed winds are only applied to the ocean) are henceforth referred to as ‘OCE’ simulations, prefixed with either a 3N or 3S to indicate the direction of wind shift (Fig. 7, right column). Similar to previous experiments, dye tracer AA-T was included once simulations had completed their 7000 year equilibration (Fig. 7). Given that we analyse changes near bottom water formation sites in Fig. 7, we show tracer concentrations after 100 years of integration only.

In simulations forced with northward shifted winds, the altered wind forcing to the ocean only (3N-OCE) results in less bottom water formation than in the fully forced experiment (3N-0) (Fig. 7a, c) as measured by the concentration of AA-T in the global ocean (6.7 % for 3N-OCE versus 9.5 % 3N-0); the new deep water formation site off the coast of Mac. Robertson Land does not switch on in simulation 3N-OCE. For simulation 3S-OCE; a decrease in sea ice around the Antarctic continent results in an increase in bottom water formation in the Weddell and Ross Seas when compared to 3S-0 (Fig. 7d, f) and is seen as an increase in AA-T concentration from 7.9 % in 3S-0 to 8.9 % in 3S-OCE. 3N-ICE and 3S-ICE simulations have similar rates of deep water formation, both lower than their respective fully forced equivalents, with AA-T concentrations of 4.2 and 4.3 % respectively after 100 years of integration. Interestingly, the new bottom water formation sites off the coast of Mac. Robertson Land and near Wilkes Land only switch on under combined dynamic forcing, suggesting the deepwater formation dynamics are highly non-linear.

While global ventilation rates increase in almost all simulations regardless of the direction of SHW shifts, the oceanic carbon budget reacts almost linearly to the shifts (Fig. 2b) with an increase in oceanic carbon for southward shifts and vice versa.

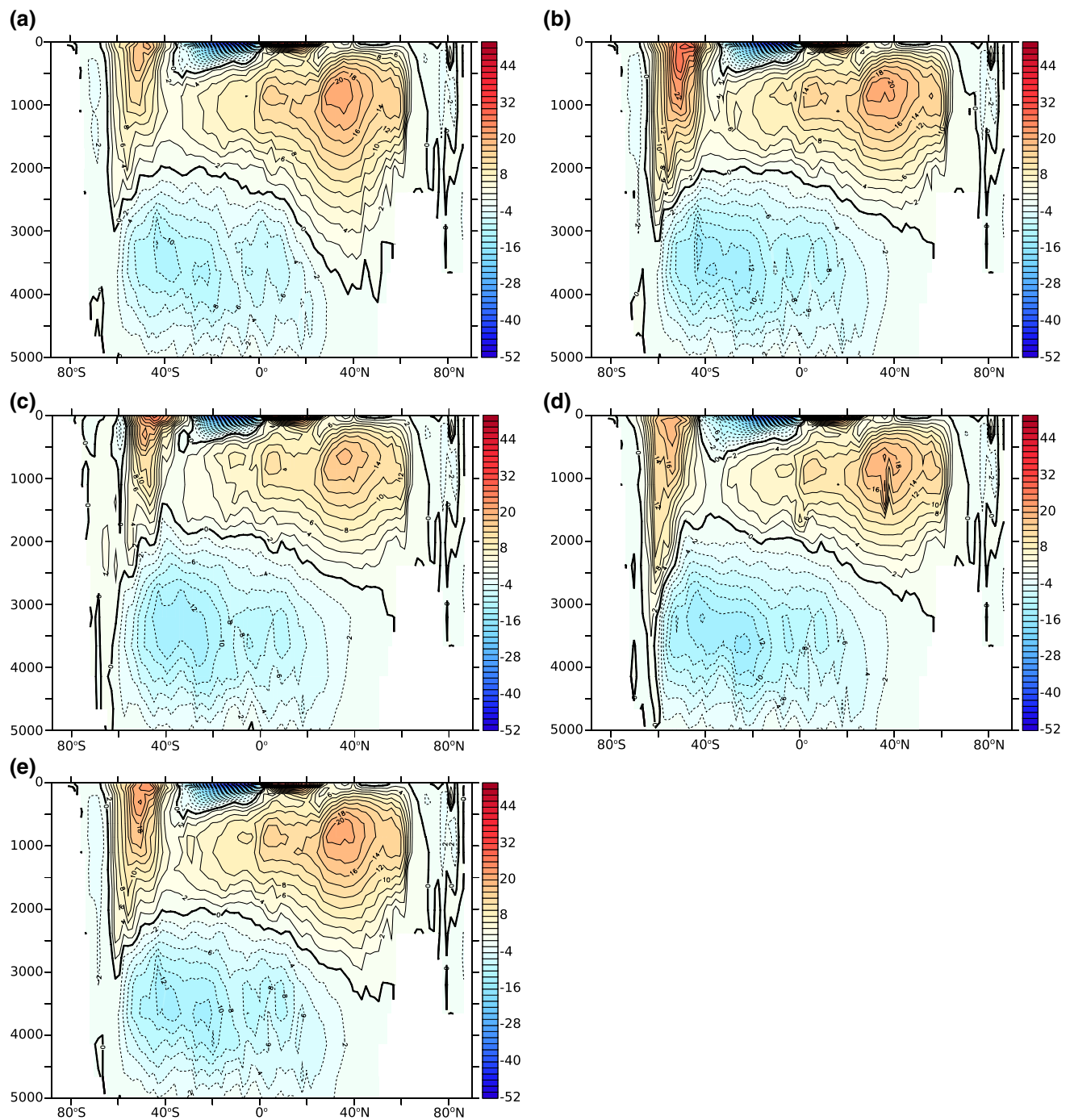


**Fig. 5** Streamfunction of zonally integrated, meridional transport plotted for simulations 0–08 (a), 0–12 (b), 3N-0 (c), 3S-0 (d) and control (e). Units are in Sverdrup

### 3.3 The physical pump

Atmospheric CO<sub>2</sub> enters the ocean via dissolution into surface waters as one of four carbonate species, collectively referred to as Dissolved Inorganic Carbon (DIC). This dissolution is dependent on the temperature and salinity of the seawater, where cooler, less saline water is able to absorb

more carbon from the atmosphere. Areas of deep water formation such as the North Atlantic and Southern Ocean are the primary regions for the subduction and advection of DIC into the ocean's interior; a process known as the physical pump. DIC in the surface ocean is also available for the soft tissue and carbonate pumps which act to export organic carbon to the deep ocean. To distinguish between

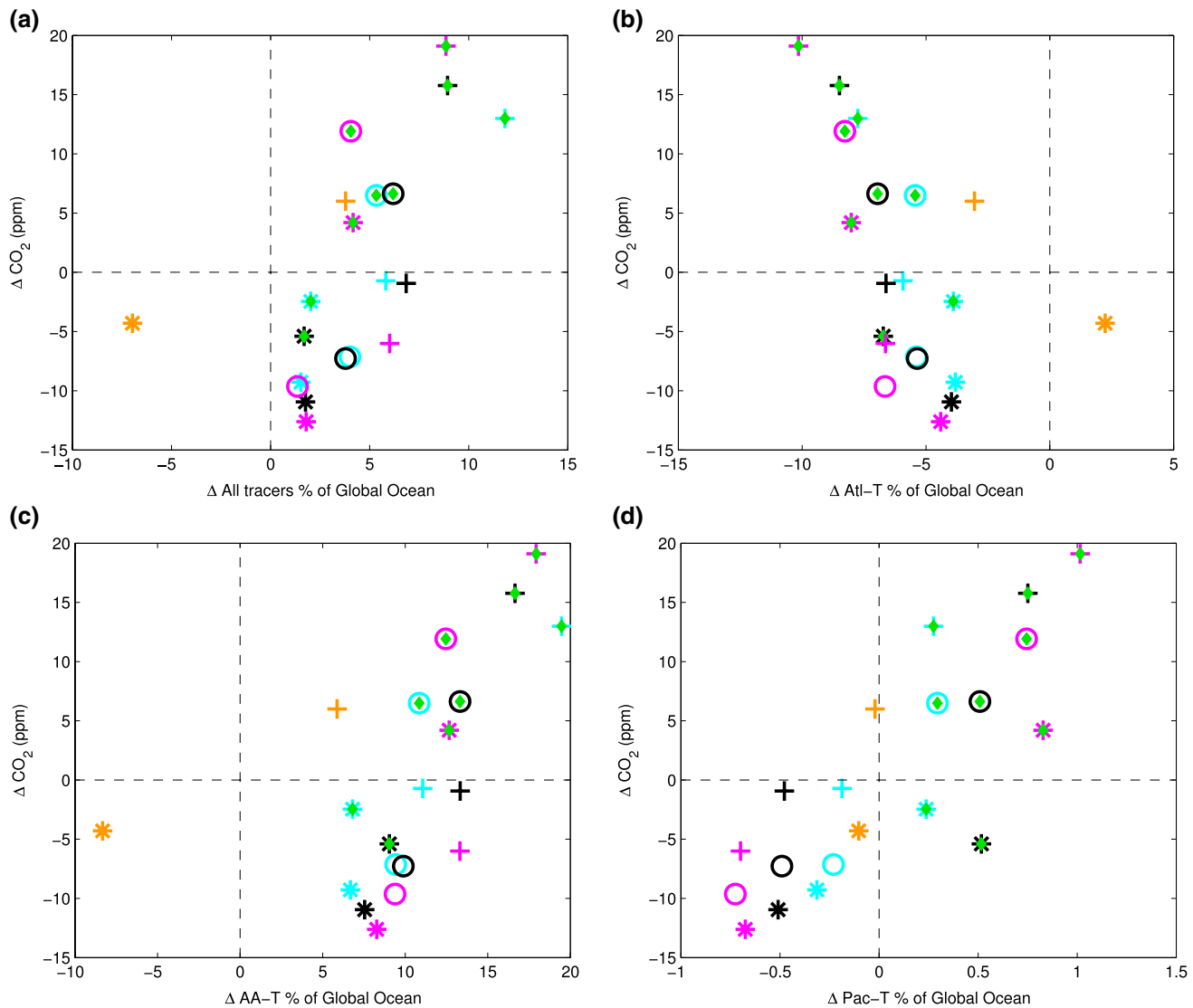


**Fig. 6** Global mean change in ocean ventilation measured as changes in dye tracer concentration (Fig. 1b). **a** Concentration of all tracers with respect to the control simulation versus changes in atmospheric  $\text{CO}_2$ , **b** North Atlantic tracer (Atl-T) concentration versus  $\text{CO}_2$ , **c** Southern Ocean tracer (AA-T) concentration versus  $\text{CO}_2$ , **d** North Pacific tracer (Pac-T) concentration versus  $\text{CO}_2$ . See Table 1 for symbols

**b** North Atlantic tracer (Atl-T) concentration versus  $\text{CO}_2$ , **c** Southern Ocean tracer (AA-T) concentration versus  $\text{CO}_2$ , **d** North Pacific tracer (Pac-T) concentration versus  $\text{CO}_2$ . See Table 1 for symbols

the biological and physical pumps, we have introduced two additional prognostic tracers into the model that explicitly track preformed and remineralised DIC. Preformed DIC is defined as carbon originating in the surface layer of the ocean via carbon exchange with the atmosphere and the upwelling of DIC into the mixed layer. It then enters the interior ocean via convection and advection in the process of water mass formation. Remineralised carbon is defined as carbon created by biological processes which subsequently remineralises at depth. These tracers were included for the full integration time of 7000 years.

The increase in ocean ventilation discussed in Sect. 3.2, primarily due to increased AABW formation, leads to an increase in preformed DIC in almost all simulations

(see Figs. 8a, 9a for simulations 3N-0 and 3S-0 as examples) caused by an increased efficiency of the physical pump (compare colours and contours in Figs. 8a, 9a). This increased efficiency of the physical pump is driven by an increase in ventilation and likely also the decrease in global ocean temperature.

### 3.4 The biological pump

The process of photosynthesis by phytoplankton in the euphotic zone utilises dissolved nutrients and inorganic carbon to create organic matter. A portion of this organic matter is exported to depth, resulting in a net export of particulate organic carbon and nutrients such as nitrate

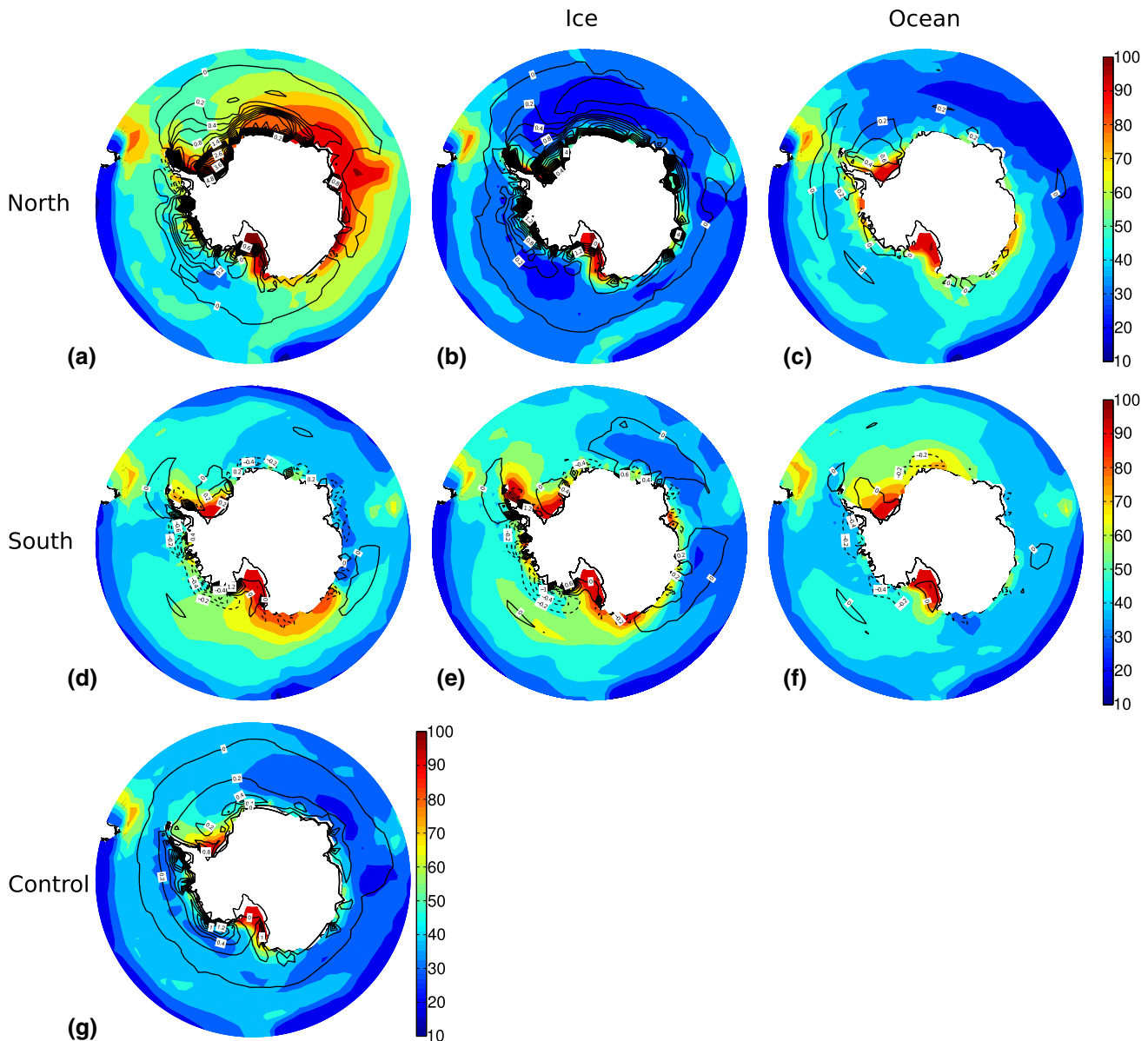


**Fig. 7** Southern Ocean tracer (AA-T) as an indicator for Antarctic bottom water formation for experiments **a** 3N-0, **b** 3N-ICE, **c** 3N-OCE, **d** 3S-0, **e** 3S-ICE, **f** 3S-OCE and **g** Control. Figures shows vertically averaged tracer concentration after 100 years of integration.

and phosphate from the surface to the interior ocean. This export via aggregation and sinking of organic detritus and subsequent remineralisation at depth is known as the soft tissue pump. Export is calculated in our model as detritus made up of deceased phytoplankton and zooplankton as well as grazed phytoplankton that is not assimilated into zooplankton, minus a fraction that is rapidly remineralised at the surface. Previous studies have examined biological activity in the ocean using different proxies, such as surface export production of carbon (Toggweiler et al. 2006; Tschemi et al. 2008; Menviel et al. 2008; d'Orgeville et al. 2010), apparent oxygen utilisation (AOU) (Doval and

Hansell 2000) and preformed/remineralised tracers for nutrients and carbon (Sarmiento et al. 2004; Ito and Follows 2005; Marinov et al. 2006; Schmittner et al. 2008, 2013).

Global mean surface export production of carbon at 240 m depth (Fig. 10a) and at 2 km depth (not shown) decreases for all but five simulations. For simulations forced with southward shifted SHW, a decrease in upwelling of nutrients at 40°S leads to a decrease in net primary production in these regions. Simulations forced with northward shifted winds see an increase in available nutrients and export production around 40°S (Fig. 10b),

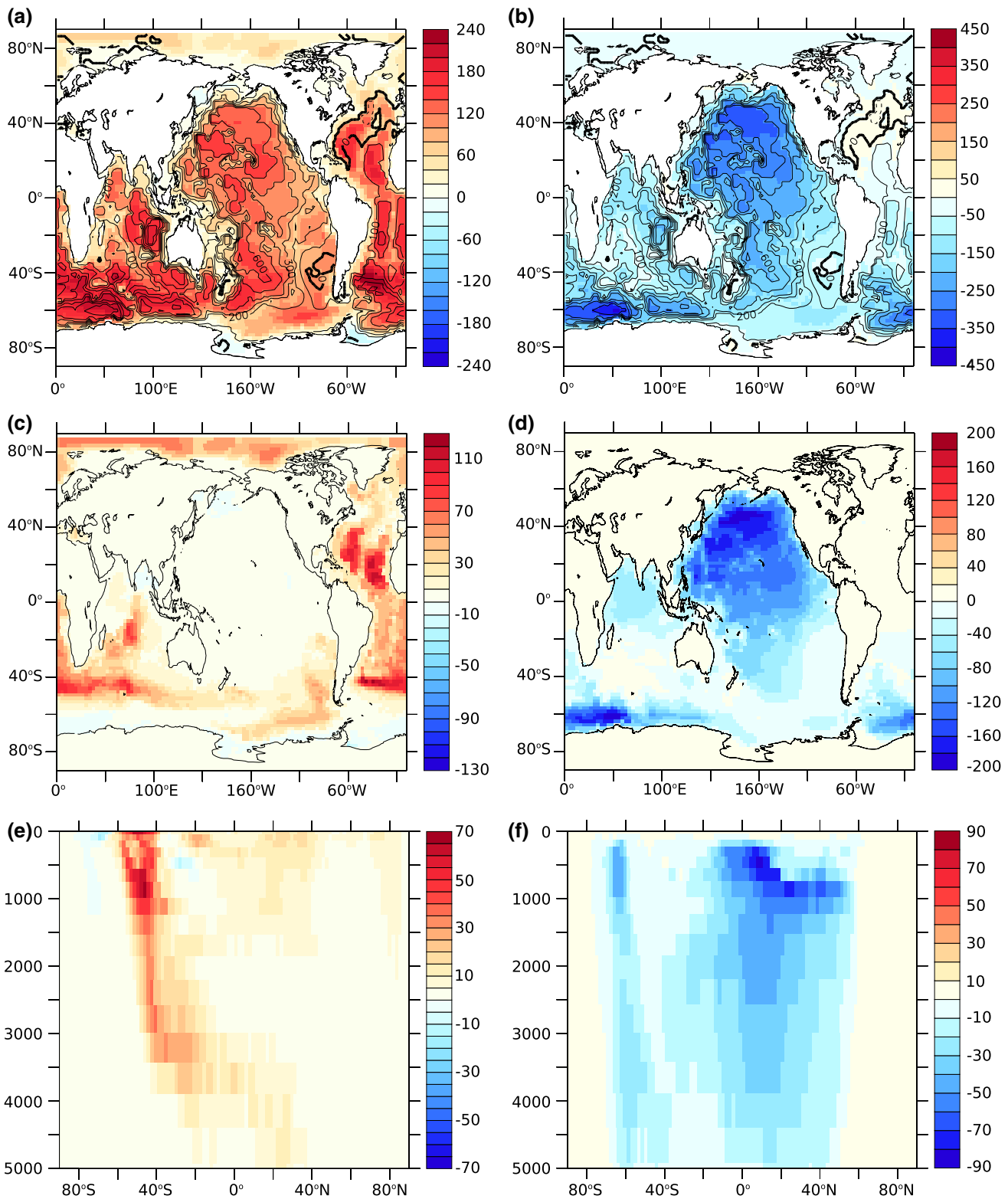


**Fig. 8** Anomalies of annual mean, vertically integrated preformed (a) and remineralised (b) DIC ( $\text{mol C m}^{-2}$ ) for simulation 3N-0, contours on both show vertically integrated, annual mean anomalies for the sum of all dye tracers. Vertically integrated anomalies in preformed (c) and remineralised (d) DIC over gridcells where the

changes in the physical pump outweigh changes in the biological pump (c) and vice versa (d). Zonally integrated changes of preformed (e) and remineralised (f) DIC over gridcells where the changes in the physical pump outweigh changes in the biological pump (e) and vice versa (f)

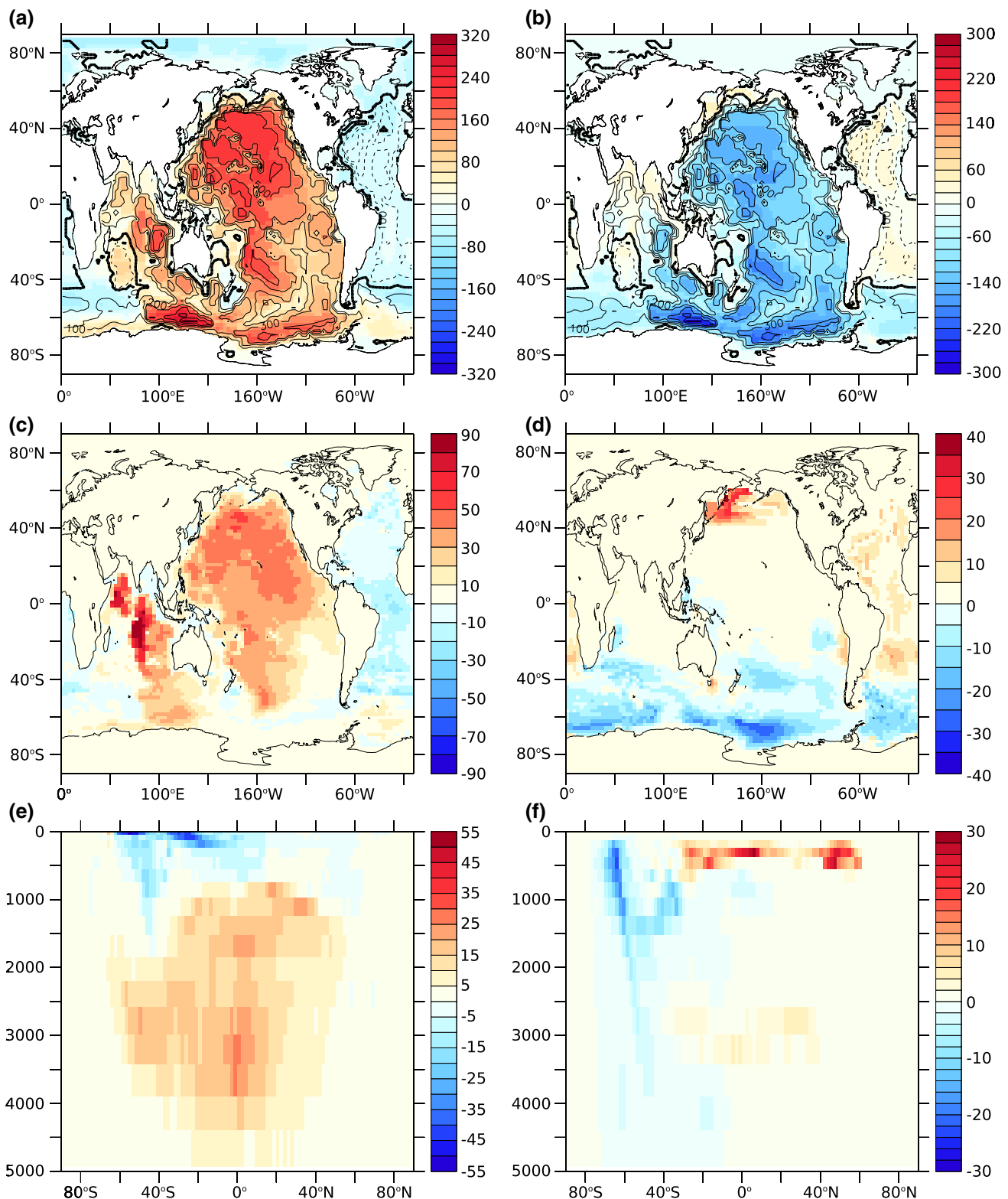


**Fig. 9** Anomalies of annual mean, vertically integrated preformed (a) and remineralised (b) DIC ( $\text{mol C m}^{-2}$ ) for simulation 3S-0, contours on both show vertically integrated, annual mean anomalies for the sum of all dye tracers. Vertically integrated anomalies in preformed (c) and remineralised (d) DIC over gridcells where the

changes in the physical pump outweigh changes in the biological pump (e) and vice versa (d). Zonally integrated changes of preformed (e) and remineralised (f) DIC over gridcells where the changes in the physical pump outweigh changes in the biological pump (e) and vice versa (f)

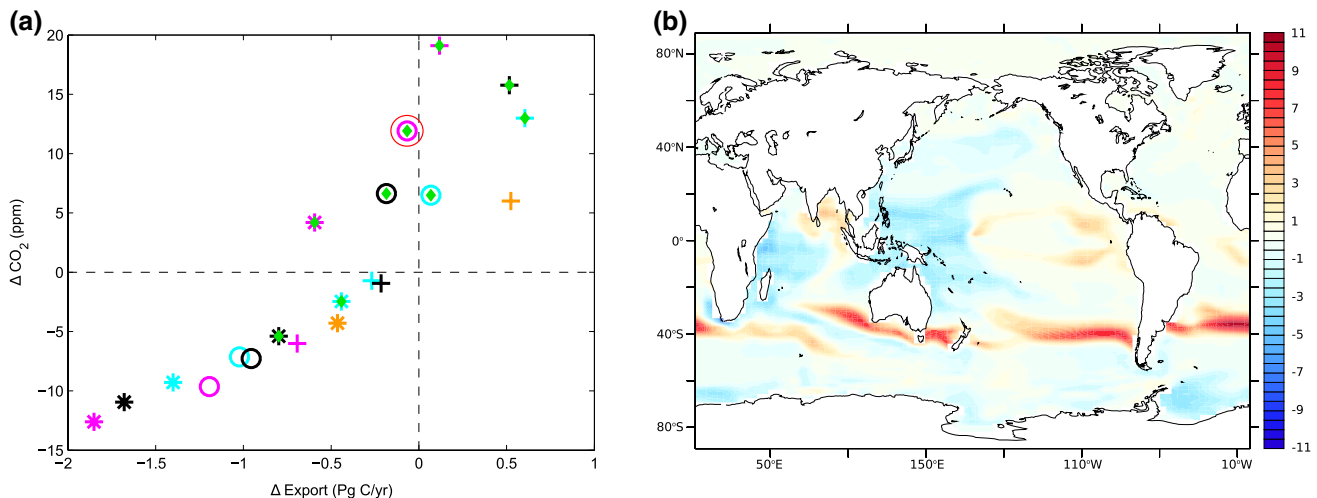


**Fig. 10** **a** Change in global surface carbon export production at 240 m versus change in atmospheric  $\text{CO}_2$ . See Table 1 for symbols. Simulation 3N-0 is highlighted for emphasis. **b** Change in annual

mean surface export production of carbon for simulation 3N-0 with respect to the control simulation ( $\text{mol C m}^{-2} \text{ year}^{-1}$ ) at 240 m depth

however export production decreases in the Indian and western Pacific basins as well as in the Southern Ocean. The concurrent global decrease in export production throughout the water column and decrease in atmospheric  $\text{CO}_2$  for our southward shifted simulations suggests that changes in export production are not the dominant mechanism for the resulting change in atmospheric carbon.

Our simulations see large changes in remineralised DIC throughout the entire ocean, particularly in regions of large dye tracer anomalies. Using simulations 3N-0 and 3S-0 as examples, we observe a notable decrease in remineralized DIC in the Southern and Pacific Oceans (Figs. 8b, 9b), which is consistent with an increase in dye tracer concentration (contours in Figs. 8b, 9b). Changes in total concentration of dye tracers measures changes in residence time, with an increase in dye tracer concentration indicating a decrease in residence time. The larger the residence time of a water mass, the more biologically fixed carbon can remineralise and accumulate, changing remineralized carbon regardless of changes in biological production and export.

As can be seen in Fig. 11a, the net decrease in ocean carbon for simulation 3N-0 is due to the depletion of remineralized DIC caused by an overall decrease in residence time (Fig. 8b) despite a considerable increase in preformed carbon (Fig. 8a). Vertically integrated preformed and remineralized DIC anomalies are generally of opposite sign (compare Fig. 8a, b).

Figure 11a shows that simulation 3N-0 is not an outlier. The increase in ocean ventilation decreases the residence time of water masses and leads to a depletion of remineralised DIC in almost all simulations. At the same time, preformed DIC increases in almost all simulations due to an increased efficiency of the physical pump. Changes in

preformed and remineralised DIC are of opposite sign for all simulations. For simulations forced with northward shifted SHW, changes in the biological pump outweigh the changes in the physical pump, leading to an increase in atmospheric  $\text{CO}_2$ . The opposite is true for southward shifts of the SHW.

### 3.5 Competition between pumps

By changing exclusively the dynamic forcing of the ocean, one would expect that the resulting changes in the carbon budgets are directly linked to changes in water masses. A globally colder and better ventilated ocean should therefore lead to a more efficient physical pump (Sect. 3.3) and a less efficient biological pump (Sect. 3.4). In our study, almost all sensitivity simulations (except 0-08) see an increase in global ventilation, and therefore an increase in globally integrated preformed carbon and a decrease in globally integrated remineralized carbon (Fig. 11a). The resulting change in the global ocean carbon budget therefore depends on which one of the two pumps wins this “tug of war”. Fig. 11a shows that changes in the biological pump outweigh changes in the physical pump for our northward shifted simulations, as well as for simulation 0-12 (the symbols lie below the  $y = -x$  line). The only exception is simulation 2N-08. For southward shifted wind forcing as well as simulation 0-08, the physical pump is winning without exception.

Figures 8c and e show vertically and zonally integrated changes in DIC for simulation 3N-0, where only grid cells are taken into account for which the absolute change in preformed DIC is of opposite sign and larger than the correspondent change in remineralized DIC. It therefore

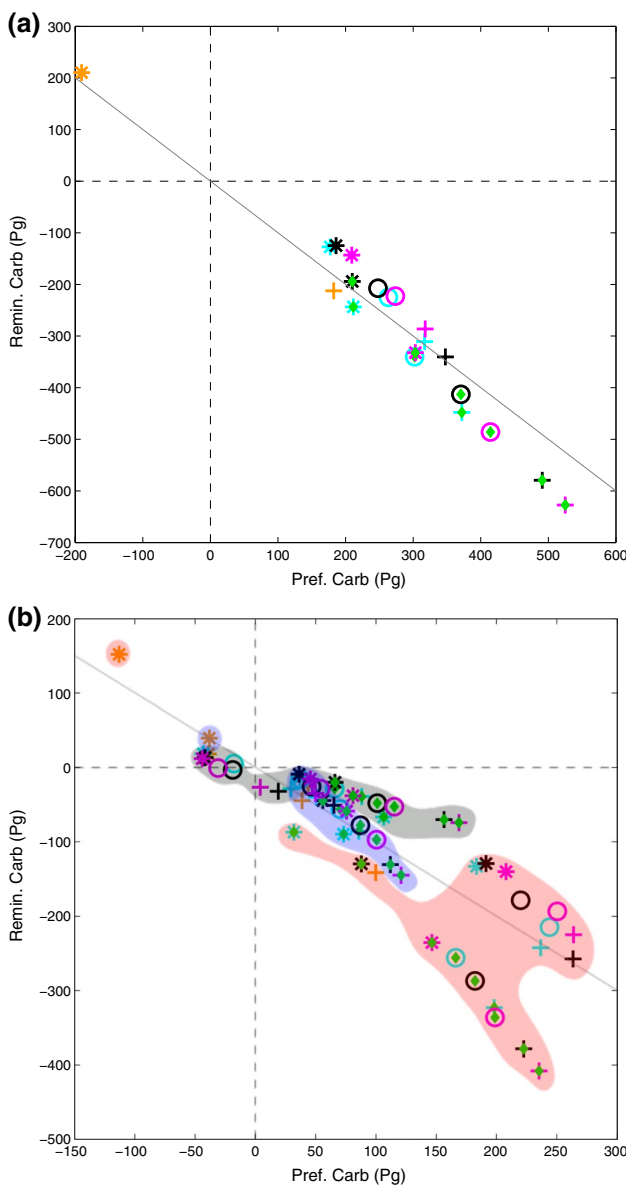


**Fig. 11** Change in globally integrated preformed versus remineralised carbon (Pg) relative to the control simulation (a);  $x = -y$  line is plotted in grey. Change in preformed versus remineralised carbon (Pg) grouped by ocean basins (b). Pacific (red), Atlantic (black), Indian (blue)

shows the regions in which changes in the physical pump outweigh changes in the biological pump. The equivalent for remineralized carbon can be seen in Fig. 8d, f. While the physical pump outcompetes the biological pump in the Atlantic and Southern Oceans north of  $60^{\circ}\text{S}$ , large parts of the Pacific, Indian and the Southern Ocean south of  $60^{\circ}\text{S}$  are governed by changes in the biological pump, a pattern similar to Fig. 3a, b.

Overall, the pattern of changes in preformed and remineralized carbon for simulation 3S-0 look similar (compare Fig. 8a, b with Fig. 9a, b). However, regions depicting the

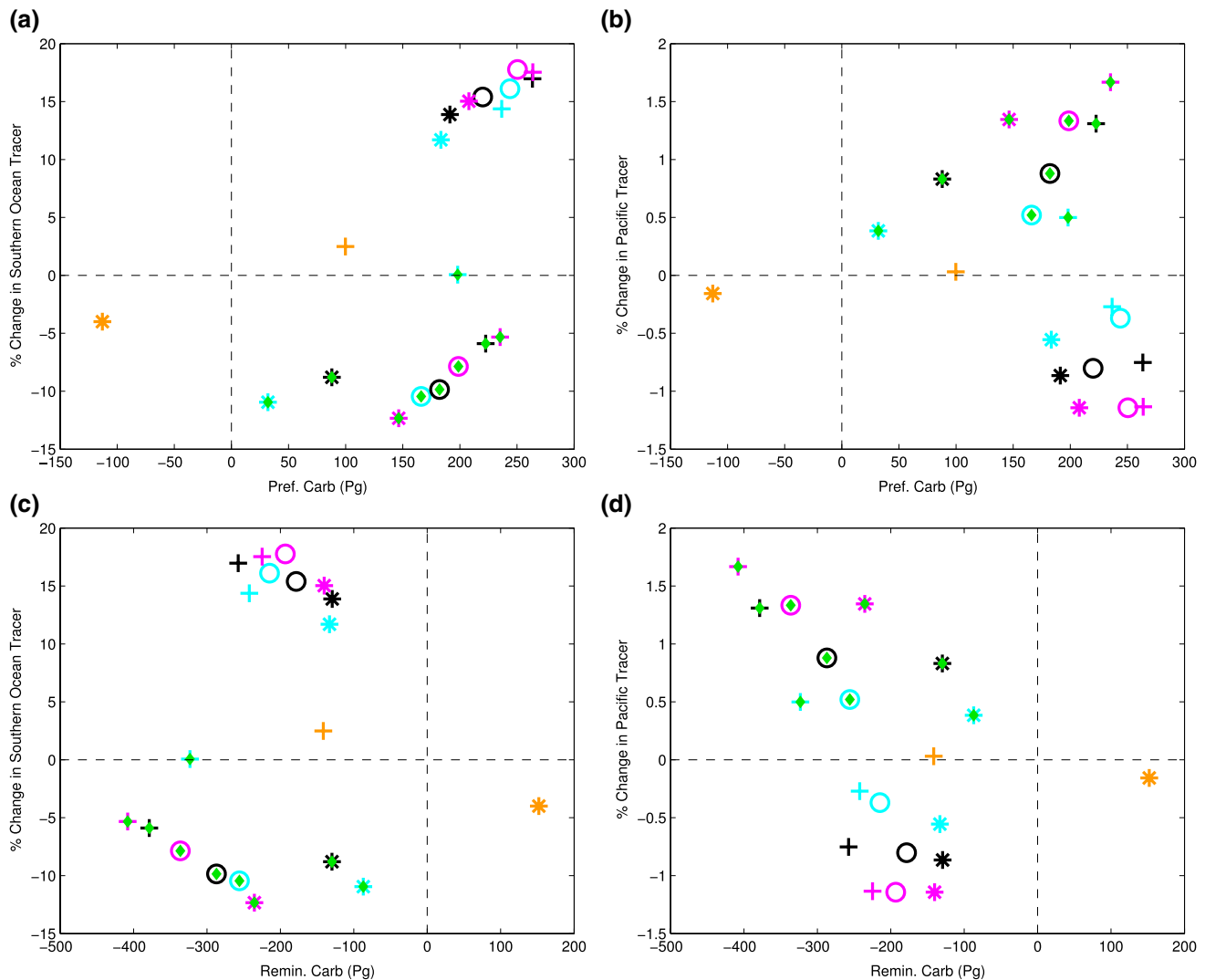
“winning” pump are very different (compare Fig. 8c, d with Fig. 9c, d). For simulation 3S-0, changes in preformed carbon outweigh changes in remineralised carbon over most of the Pacific and Indian Oceans, while changes in remineralised carbon are mostly dominant in the Southern Ocean; again, a pattern similar to Fig. 3c, d.

Figure 11b shows changes in remineralised and preformed carbon for all ocean basins and all simulations. Given the size of the Pacific Ocean, the global carbon budgets are mainly dictated by changes seen in the Pacific Basin. While the main active water masses in the Pacific Ocean are AABW and AAIW, there is a small source of North Pacific sourced water (Fig. 6d) with global concentration changes of about one order of magnitude smaller than for other water masses.

Figure 12a and c shows changes in preformed and remineralised DIC versus changes in southern sourced water masses in the Pacific basin. Simulations forced with southward shifted winds, as well as simulations forced with no shifts (0–08 and 0–12), show the expected pattern where increased ventilation leads to an increase in preformed and a decrease in remineralised carbon and vice-versa. This is in accordance with Fig. 9c, e, where changes due to the “winning” physical pump in the deep Pacific Ocean are mainly caused by changes in AABW, with changes seen below a depth of 1000 m (Fig. 9e). However, for simulations forced with northward shifted winds, the changes in carbon budgets are not consistent with changes in AABW (Fig. 12a, c); instead they are consistent with changes in North Pacific sourced water (Fig. 12b, d). This is in accordance with Fig. 8d, f, where the largest changes due to the “winning” biological pump in the Pacific Ocean are shallower than for simulations forced with southward shifted winds (compare Fig. 8f, 9e).

Figure 13 shows changes in DIC integrated over each ocean basin as a function of changes in atmospheric  $\text{CO}_2$  (a) and atmospheric  $\Delta^{14}\text{CO}_2$  (b), for all simulations. The sign and steepness of the slopes for each ocean basin ensemble shows that changes in the carbon reservoir of the Pacific Ocean dictate the changes felt by the atmosphere. For example, the  $\Delta \text{DIC}/\Delta^{14}\text{CO}_2$  slope is negative for the Atlantic and positive for the Pacific Ocean, therefore atmospheric  $\Delta^{14}\text{CO}_2$  increases when the Atlantic ocean is losing and the Pacific Ocean is gaining carbon. Furthermore, the  $\Delta \text{DIC}/\Delta \text{CO}_2$  slope is steeper for the Pacific ensemble than for the Atlantic; it is positive for the Atlantic and negative for the Pacific Ocean.

In summary, changes in the global ocean carbon budget are mainly governed by changes in the Pacific Ocean. In the Pacific Ocean, two different regimes crystallize in our simulations: for simulations forced with southward shifted winds an increase in southern sourced water masses enhances the physical pump and weakens the biological



**Fig. 12** Carbon budgets in the Pacific Ocean. Change in preformed carbon versus change in Southern Ocean tracer (AA-T) concentration (a); preformed carbon versus change in North Pacific tracer (PAC-T)

concentration (b); remineralised carbon versus AA-T (c); and remineralised carbon versus PAC-T (d)

pump, leading overall to an increase in DIC (with the physical pump winning the “tug-of-war”). For simulations forced with northward shifted winds a slight increase in northern sourced water masses enhances the physical pump and weakens the biological pump, leading overall to an decrease in DIC (with the biological pump winning the “tug-of-war”).

#### 4 Discussion

We find that an increase in the intensity of the SHW results in increased atmospheric CO<sub>2</sub> and vice versa, in line with Russell et al. (2006), Tschumi et al. (2008), d’Orgeville et al. (2010). Contrary to d’Orgeville et al. (2010) and

Völker and Köhler (2013) however, changes in latitude of the SHW have a non-negligible impact on atmospheric CO<sub>2</sub> in our simulations; with a northward shift resulting in an increase in CO<sub>2</sub> and vice versa. Simulations forced with shifted SHW and no change in intensity undergo a larger change in atmospheric Δ<sup>14</sup>C and CO<sub>2</sub> than simulations forced with a 20 % change in intensity and no shift (Fig. 2).

Völker and Köhler (2013) integrate simulations with the MITgcm under Last Glacial Maximum boundary conditions forced with latitudinal shifts of the SHW by 10°. The change in zonally integrated DIC in their simulations (their Fig. 12) is similar to our simulations 3N-0 and 3S-0. Both models simulate a decrease in DIC along the AABW pathway and an increase in the upper ocean, with a maximum DIC change around 40°S for northward shifted winds

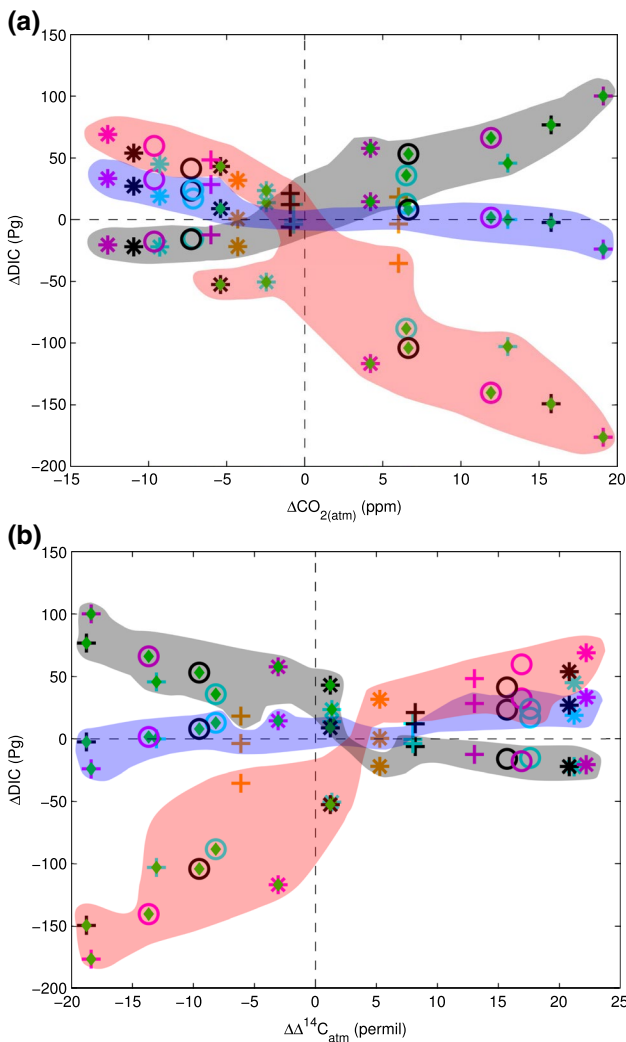


**Fig. 13** Changes in Dissolved Inorganic Carbon (DIC) are plotted against changes in atmospheric CO<sub>2</sub> (a) and changes in atmospheric  $\Delta^{14}\text{CO}_2$  (b) for the Atlantic (black), Indian (blue) and Pacific (red) basins

and the opposite for simulations forced with a southward shift of the SHW. The main difference between the two studies can be seen in the shallow North Pacific Ocean (within the first 1500 m), where the UVic ESCM simulates significant changes in DIC that are not seen in the simulations with the MITgcm. The different behaviour of the North Pacific might explain why, contrary to our results, Völker and Köhler (2013) find an increase in CO<sub>2</sub> for both a north- and south-ward shift of the SHW, although DIC changes are similar in both studies over most of the world's ocean. Simulations integrated with LOVECLIM forced with wind intensity changed by  $\pm 15\%$  show DIC changes in the upper 3000 m of the Pacific Ocean similar to our simulations 0–12 and 0–08 (Meniel et al. (2008), their Fig. 7). However, a decrease in wind intensity leads

to an accumulation of carbon in the deep Pacific Ocean (below 3000 m) that we do not see in our simulations. The impact on atmospheric CO<sub>2</sub> is also comparable with our results, both studies find an increase in atmospheric CO<sub>2</sub> by  $\sim 5$  ppm for simulations forced with increased intensity, and a decrease by  $\sim 5$  ppm for a weakening of the SHW. A relatively large increase in atmospheric CO<sub>2</sub> of 20 ppm is found by Lauderdale et al. (2013) in simulations with the MITgcm for northward shifted or stronger SHW, and the opposite for a southward shift or weaker SHW. These results agree qualitatively with our study, although changes in intensity appear to have a larger impact on the ocean carbon budget in their simulations than in our simulations, while shifts appear to have a larger impact in our simulations. Zonally integrated changes in DIC (their Fig. 5) compare well for changes in intensity (our simulations 0–12 and 0–08), as well as for simulations forced with northward shifted winds (our simulation 3N-0). The upper 2000 m for the southward shifted simulations (our simulation 3S-0) also compare well, while the deep ocean (below 2000 m) is of opposite sign in our simulation.

Interestingly, with the exception of simulation 0–08, all of our simulations show an increase in Southern Ocean sourced water masses and an increase in global ventilation with a concurrent decrease in global mean ocean temperature. The efficiency of the physical pump increases, leading to a net increase in preformed carbon. It should be noted that without deconstructing preformed carbon into its base components ( $\text{DIC}_{\text{pref}} = \text{DIC}_{\text{sat}} + \text{DIC}_{\text{dis}}$ ), it is not possible to determine the precise impact a change in surface temperature has on preformed DIC. At the same time, the increase in ventilation leads to a decrease in residence time and therefore a decrease in the efficiency of the biological pump. Overall, the net changes in remineralised and preformed carbon almost balance each other out, given that both are due to the same underlying change in ocean dynamics (Fig. 11a).

Changes in ocean residence times, particularly in the Pacific Ocean, are the dominant mechanism responsible for the changes seen in atmospheric CO<sub>2</sub> in our model. Given the non-linear response of ocean dynamics to wind forcing, caution should be taken when analysing and comparing studies with different climate models or slightly different forcing. This is particularly relevant to the previous studies by Huiskamp and Meissner (2012) and Meniel et al. (2014), both of which demonstrate vigorous deep water formation in the North Pacific under glacial or near-glacial boundary conditions. However, circulation changes described here are restricted to the top 1000 m of the ocean and are of the order of magnitude of 1 Sv or less. A closer comparison can be made to Tschumi et al. (2008) who find that upper North Pacific overturning is particularly sensitive to latitudinal shifts of the westerlies. Their finding agrees with ours; a northward shift enhances this surface

overturning while changes in the deep Pacific are almost negligible. Instead of inferring that similar changes in wind forcing will have similar effects on the global carbon cycle for different climate models, a thorough analysis of changes in water masses and circulation is warranted.

## 5 Conclusion

In this study we have demonstrated that a combination of shifts in latitude and changes in intensity of the Southern Hemisphere westerlies (SHW) leads to an exchange of carbon between the ocean and atmosphere, driven primarily by changes in ocean ventilation and the competing efficiencies of the physical and biological pumps. We find that changes in the Pacific Ocean carbon budgets dictate the overall changes in global marine and atmospheric carbon. Southward shifted SHW lead to a decrease in atmospheric CO<sub>2</sub> in our simulations, caused by increased efficiency of the physical pump while simulations with northward shifted SHW resulting in an increase in atmospheric CO<sub>2</sub> caused by a decreased efficiency of the biological pump. We find that changes in ocean circulation are highly non-linear and therefore caution should be taken when directly linking changes in atmospheric CO<sub>2</sub> to changes in dynamic forcing. The air-sea carbon exchange is partially offset by the terrestrial biosphere's response to the change in atmospheric CO<sub>2</sub> in all our simulations, similar to Zickfeld et al. (2007) and Menzel et al. (2008).

**Acknowledgments** The authors would like to thank Matthew England, Chris Turney and Paul Valdes for comments on earlier drafts of this manuscript. The work was supported by the Australian Research Council (FT100100443, DP130104156). KJM is grateful for an award under the Merit Allocation Scheme on the NCI National Facility at the ANU. The authors declare that they have no conflict of interest.

## References

- Archer D (1996) A data-driven model of the global calcite lysocline. *Global Biogeochem Cycles* 10(3):511–526
- Berger AL (1978) Long-term variations of daily insolation and quaternary climatic changes. *J Atmos Sci* 35:2362–2367
- Biastoch A, Böning CW, Schwarzkopf FU, Lutjeharms JRE (2009) Increase in Agulhas leakage due to poleward shift of Southern Hemisphere westerlies. *Nature* 462:495–498. doi:[10.1038/nature08519](https://doi.org/10.1038/nature08519)
- Bryan K, Lewis LJ (1979) A water mass model of the World Ocean. *J Geophys Res Oceans* 84(C5):2503–2517. doi:[10.1029/JC084iC05p02503](https://doi.org/10.1029/JC084iC05p02503)
- Chen G, Millero FJ (1979) Gradual increase of oceanic CO<sub>2</sub>. *Nature* 277:205–206
- Delworth TL, Zeng F (2008) Simulated impact of altered Southern Hemisphere winds on the Atlantic meridional overturning circulation. *Geophys Res Lett* 35(20). doi:[10.1029/2008GL035166](https://doi.org/10.1029/2008GL035166)
- d'Orgeville M, Sijp WP, England MH, Meissner KJ (2010) On the control of glacial-interglacial atmospheric CO<sub>2</sub> variations by the Southern Hemisphere westerlies. *Geophys Res Lett* 37(21):1–5
- Doval M, Hansell DA (2000) Organic carbon and apparent oxygen utilization in the western South Pacific and the central Indian Oceans. *Mar Chem* 68(3):249–264. doi:[10.1016/S0304-4203\(99\)00081-X](https://doi.org/10.1016/S0304-4203(99)00081-X). <http://www.sciencedirect.com/science/article/pii/S03044203990081X>
- Eby M, Zickfeld K, Montenegro A, Archer D, Meissner KJ, Weaver AJ (2009) Lifetime of anthropogenic climate change: millennial time-scales of potential CO<sub>2</sub> and surface temperature perturbations. *J Clim* 22:2501–2511. doi:[10.1175/2008JCLI2554.1](https://doi.org/10.1175/2008JCLI2554.1)
- Gent P, McWilliams J (1990) Isopycnal mixing in ocean circulation models. *J Phys Oceanogr* 20:150–155
- Hibler III WD (1979) A dynamic thermodynamic sea ice model. *J. Phys. Oceanogr.* 9(4):815–846. [http://journals.ametsoc.org/doi/abs/10.1175/1520-0485\(1979\)00%9%3C0815%3AADTSIM%3E2.0.CO%3B2](http://journals.ametsoc.org/doi/abs/10.1175/1520-0485(1979)00%9%3C0815%3AADTSIM%3E2.0.CO%3B2)
- Huiskamp WN, Meissner KJ (2012) Oceanic carbon and water masses during the mystery interval: A model-data comparison study. *Paleoceanography* 27:PA4206. doi:[10.1029/2012PA002368](https://doi.org/10.1029/2012PA002368)
- Hunke EC, Dukowicz JK (1997) An elastic-viscous-plastic model for sea ice dynamics. *J Phys Oceanogr* 27(9):1849–1867
- Ito T, Follows M (2005) Preformed phosphate, soft tissue pump and atmospheric CO<sub>2</sub>. *J Mar Res* 63:813–839. doi:[10.1357/0022240054663231](https://doi.org/10.1357/0022240054663231)
- Kalnay E, Kanamitsu M, Kistler R, Collins W, Deaven D, Gandin L, Iredell M, Saha S, White G, Woollen J, Zhu Y, Chelliah M, Ebisuzaki W, Higgins W, Janowiak J, Mo KC, Ropelewski C, Wang J, Leetma A, Reynolds R, Jenne R, Joseph D (1996) The NCEP/NCAR 40-year reanalysis project. *Bull Am Meteorol Soc* 77(3):437–471
- Lauderdale JM, Garabato ACN, Oliver KI, Follows MJ, Williams RG (2013) Wind-driven changes in Southern Ocean residual circulation, ocean carbon reservoirs and atmospheric CO<sub>2</sub>. *Clim Dyn* 41(7–8):2145–2164. doi:[10.1007/s00382-012-1650-3](https://doi.org/10.1007/s00382-012-1650-3)
- Lee S, Feldstein SB (2013) Detecting ozone- and greenhouse gas-driven wind trends with observational data. *Science* 339(6119):563–567. doi:[10.1126/science.1225154](https://doi.org/10.1126/science.1225154). <http://www.sciencemag.org/content/339/6119/563.full.pdf>
- Lovenduski NS, Ito T (2009) The future evolution of the Southern Ocean CO<sub>2</sub> sink. *J Mar Res* 67(5):597–617. doi:[10.1357/002224009791218832](https://doi.org/10.1357/002224009791218832)
- Lovenduski NS, Gruber N, Doney SC, Lima ID (2007) Enhanced CO<sub>2</sub> outgassing in the Southern Ocean from a positive phase of the Southern Annular Mode. *Global Biogeochem Cycles* 21(2):gb2026. doi:[10.1029/2006GB002900](https://doi.org/10.1029/2006GB002900)
- Marinov I, Gnanadesikan A, Toggweiler JR, Sarmiento JL (2006) The Southern Ocean biogeochemical divide. *Nature* 441:964–967. doi:[10.1038/nature04883](https://doi.org/10.1038/nature04883)
- Marshall J, Speer K (2012) Closure of the meridional overturning circulation through Southern Ocean upwelling. *Nat Geosci* 5(3):171–180
- McDermott DA (1996) The regulation of northern overturning by Southern Hemisphere winds. *J Phys Oceanogr* 26(7):1234–1255. doi:[10.1175/1520-0485\(1996\)026<1234:TRONOB>2.0.CO;2](https://doi.org/10.1175/1520-0485(1996)026<1234:TRONOB>2.0.CO;2)
- Meissner K, Weaver A, Matthews H, Cox P (2003a) The role of land surface dynamics in glacial inception: a study with the UVic earth system model. *Clim Dyn* 21(7–8):515–537. doi:[10.1007/s00382-003-0352-2](https://doi.org/10.1007/s00382-003-0352-2)
- Meissner KJ (2007) The Younger Dryas: a data to model comparison to constrain the strength of the overturning circulation. *Geophys Res Lett* 34(L21):705
- Meissner KJ, Schmittner A, Weaver AJ, Adkins JF (2003b) Ventilation of the North Atlantic Ocean during the Last Glacial Maximum: a comparison between simulated and observed radiocarbon ages. *Paleoceanography* 18(2). doi:[10.1029/2002PA000762](https://doi.org/10.1029/2002PA000762)
- Meissner KJ, McNeil BI, Eby M, Wiebe EC (2012) The importance of the terrestrial weathering feedback for multimillennial coral reef habitat recovery. *Global Biogeochem Cycles* 26(3):GB3017. doi:[10.1029/2011GB004098](https://doi.org/10.1029/2011GB004098)

- Menviel L, Timmermann A, Mouchet A, Timm O (2008) Climate and marine carbon cycle response to changes in the strength of the Southern Hemispheric westerlies. *Paleoceanography* 23(4). doi:10.1029/2008PA001604
- Menviel L, England MH, Meissner KJ, Mouchet A, Yu J (2014) Atlantic-Pacific seesaw and its role in outgassing CO<sub>2</sub> during Heinrich events. *Paleoceanography* 29(1):58–70. doi:10.1002/2013PA002542
- Munday DR, Johnson HL, Marshall DP (2014) Impacts and effects of mesoscale ocean eddies on ocean carbon storage and atmospheric pCO<sub>2</sub>. *Global Biogeochem Cycles* 28(8):877–896. doi:10.1002/2014GB004836
- Pacanowski RC (1995) MOM 2 documentation, user's guide and reference manual. In: Technical Report 3, GFDL Ocean Group, Geophysical Fluid Dynamics Laboratory, Princeton, USA
- Previtali M, Polvani LM (2014) Climate system response to stratospheric ozone depletion and recovery. *Q J R Meteorol Soc*. doi:10.1002/qj.2330
- Rahmstorf S, England MH (1997) Influence of Southern Hemisphere winds on North Atlantic deep water flow. *J Phys Oceanogr* 27(9):2040–2054
- Russell JL, Dixon KW, Gnanadesikan A, Stouffer RJ, Toggweiler JR (2006) The southern hemisphere westerlies in a warming world: propping open the door to the deep ocean. *J Clim* 19(24):6382–6390. doi:10.1175/JCLI3984.1
- Saenko OA, Weaver AJ, Schmittner A (2003) Atlantic deep circulation controlled by freshening in the Southern Ocean. *Geophys Res Lett* 30(14). doi:10.1029/2003GL017681
- Sarmiento JL, Gruber N, Brzezinski MA, Dunne JP (2004) High-latitude controls of thermocline nutrients and low latitude biological productivity. *Nature* 427:56–60. doi:10.1038/nature02127
- Sasse TP, McNeil BI, Abramowitz G (2013) A new constraint on global air-sea CO<sub>2</sub> fluxes using bottle carbon data. *Geophys Res Lett* 40(8):1594–1599. doi:10.1002/grl.50342
- Schartau M, Oschlies A (2003) Simultaneous data-based optimization of a 1D-ecosystem model at three locations in the North Atlantic Ocean: Part 2. Standing stocks and nitrogen fluxes. *J Mar Res* 61(6):795–821
- Schmittner A, Oschlies A, Matthews HD, Galbraith ED (2008) Future changes in climate, ocean circulation, ecosystems, and biogeochemical cycling simulated for a business-as-usual CO<sub>2</sub> emission scenario until year 4000 AD. *Global Biogeochem Cycles* 22(1):GB1013
- Schmittner A, Gruber N, Mix AC, Key RM, Tagliabue A, Westberry TK (2013) Biology and air-sea gas exchange controls on the distribution of carbon isotope ratios ( $\delta^{13}\text{C}$ ) in the ocean. *Biogeosciences* 10:5793–5816. doi:10.5194/bg-10-5793-2013
- Semtner AJJ (1976) A model for the thermodynamic growth of sea ice in numerical investigations of climate. *J Phys Oceanogr* 6(3):379–389
- Sijp WP, England MH (2008) The effect of a northward shift in the southern hemisphere westerlies on the global ocean. *Prog Oceanogr* 79:1–19
- Sijp WP, England MH (2009) Southern hemisphere westerly wind control over the ocean's thermohaline circulation. *J Clim* 22(5):1277–1286
- Skinner LC, Fallon S, Waelbroeck C, Michel E, Barker S (2010) Ventilation of the deep Southern Ocean and deglacial CO<sub>2</sub> rise. *Science* 328(5982):1147–1151
- Son SW, Polvani LM, Waugh DW, Akiyoshi H, Garcia R, Kushner D, Pawson S, Rozanov E, Shepherd TG, Shibata K (2008) The impact of stratospheric ozone recovery on the southern hemisphere westerly jet. *Science* 320(5882):1486–1489. doi:10.1126/science.1155939. <http://www.science.org/content/320/5882/1486.full.pdf>
- Stuiver M, Polach HA (1977) Discussion: reporting of 14C data. *Radiocarbon* 19(3):355–363. <http://www.radiocarbon.org/Pubs/Stuiver/Stuiver-Polach.pdf>
- Swart NC, Fyfe JC, Saenko OA, Eby M (2014) Wind-driven changes in the ocean carbon sink. *Biogeosciences* 11(21):6107–6117. doi:10.5194/bg-11-6107-2014. <http://www.biogeosciences.net/11/6107/2014/>
- Takahashi T, Sweeney C, Hales B, Chipman D, Newberger T, Goddard J, Iannuzzi R, Sutherland S (2012) The changing carbon cycle in the Southern Ocean. *Oceanography* 25(3):26–37. doi:10.5670/oceanog.2012.71
- Toggweiler J, Samuels B (1995) Effect of Drake passage on the global thermohaline circulation. *Deep Sea Res Part I Oceanogr Res Pap* 42(4):477–500. doi:10.1016/0967-0637(95)00012-U. <http://www.sciencedirect.com/science/article/pii/096706379500012U>
- Toggweiler JR, Russell JL, Carson SR (2006) Midlatitude westerlies, atmospheric CO<sub>2</sub>, and climate change during the ice ages. *Paleoceanography* 21(2):PA001,154
- Tschumi T, Joos F, Parekh P (2008) How important are Southern Hemisphere wind changes for low glacial carbon dioxide? A model study. *Paleoceanography* 23(4). doi:10.1029/2008PA001592
- Völker C, Köhler P (2013) Responses of ocean circulation and carbon cycle to changes in the position of the Southern Hemisphere westerlies at Last Glacial Maximum. *Paleoceanography* 28(4):726–739. doi:10.1002/2013PA002556
- Weaver A, Hughes TMC (1992) Stability and variability of the thermohaline circulation and its link to climate. In: Jacob A (ed) Trends in physical oceanography. Research Trends Series, vol 1. Council of Scientific Research Integration, Trivandrum, India, pp 15–70
- Weaver AJ, Eby M, Wiebe EC, Bitz CM, Duffy PB, Ewen TL, Fanning AF, Holland MM, MacFadyen A, Matthews HD, Meissner KJ, Saenko O, Schmittner A, Wang H, Yoshimori M (2001) The UVic earth system climate model: model description, climatology, and applications to past, present and future climates. *Atmos Ocean* 4:361–428
- Zickfeld K, Fyfe JC, Saenko OA, Eby M, Weaver AJ (2007) Response of the global carbon cycle to human-induced changes in southern hemisphere winds. *Geophys Res Lett* 34(12). doi:10.1029/2006GL028797 Wind stress fields of the Southern Hemisphere Westerlies (SHW) are shifted northward, southward or remain in their present day location. The intensity of the field is either increased or decreased by 20 %, or remains at present day values